10.2514/6.2014-0852

AIAA SciTech Forum
13-17 January 2014, National Harbor, Maryland
55th AIAA/ASME/ASCE/AHS/ASC Structures, Structural Dynamics, and Materials Conference

Single Edge Notch Tension Test on Cross-Ply Laminated Composites for Intralaminar Fracture Properties

Stewat Boyd[1] Ashith P. K. Joseph[2] and Anthony M. Waas[3]
University of Michigan, Ann Arbor, MI, 48109

Wooseok Ji[4]
Ulsan National Institute of Science and Technology, Ulsan, S. Korea

A systematic yet simple way to measure the fracture toughness value for a Mode I crack that occurs perpendicular to the fiber direction in a unidirectional composite is presented. Cross-ply single edge notch tension (SENT) tests combined with finite element analysis areutilized to obtain the in-plane fracture toughness value under tension in the direction of fibers. The notch length of the SENT specimen is used as a parameter to back out the fracture toughness value in a consistent manner.

I. Introduction

Interlaminar fracture in polymer matrix composite (PMC) laminates, often called delamination, is defined as an out-of-plane discontinuity between two adjacent plies of a laminate. Delamination behavior has been studied by many researchers and now can be characterized in a standardized manner. Fracture properties of Mode I, Mode II, and mixed-mode (between Mode I and Mode II) delamination can be obtained from standard tests in conjunction with finite element analysis (FEA). However, a systematic approach to quantify and measure intralaminar fracture properties is not available in the literature. This presentation pertains to the development of a suitable test-analysis protocol to obtain such toughness values that can be used in virtual tests.

Intralaminar cracks are defined as in-plane discontinuities that advance through the entire laminate thickness in the direction parallel to the fiber direction. Intralaminar fracture modes are typically characterized as three major intralaminar failure mechanisms, which are distinct from the microdamage mode. They are transverse (Mode I) matrix cracking, shear (Mode II) matrix cracking, and axial (Mode I) fiber fracture as shown in Figure 1. These fracture modes are consistent with the in-plane failure typically observed in PMC laminates. The interlaminar cracks, once initiated, can trigger other failure mechanisms such as delamination and/or act as delamination migration pathways between adjacent interfaces, leading to the further growth of the delamination. Presence of such damage can cause significant reduction of the overall performance of structural components and thus, an accurate measurement and quantification of the fracture modes are fundamental to the understanding of the onset, growth, and interaction of interlaminar and intralaminar cracks. However, this activity cannot occur in isolation of the subsequent modeling effort and use of finite-element based structural analysis.

This presentation will describe a combined experimental and numerical study to provide a systematic and reliable way for measuring the intralaminar fracture properties. Especially, the fracture toughness value for the Mode I fiber failure will be obtained from single edge notch tension (SENT) tests combined with FEA simulation. It is assumed that the fracture toughness value for Mode I trasverse cracking is the same as the value for the interlaminar Mode I fracture and the vaue for shear Mode II matrix cracking is the same as the vaue for the interlaminar Mode II fracture. SENT specimens are designed to have different notch lengths with the same dimensions elsewhere in order to control the main in-plane fracture mode. The measured experimental force-displacement data, converted to a suitable stress-strain response will be compared to corresponding FEA simulations to back out the individual intralaminar fracture properties.

---

[1] Graduate Student Research Assistant, Department of Aerospace Engineering, 2038 FXB
[2] Graduate Student Research Assistant, Department of Aerospace Engineering, 2038 FXB
[3] Felix Pawlowski Collegiate Professor, Department of Aerospace Engineering, 3044 FXB, Fellow of AIAA.
[4] Assistant Professor, School of Mechanical and Advanced Materials Engineering, 301-7 Engineering Building #1, Member of AIAA.

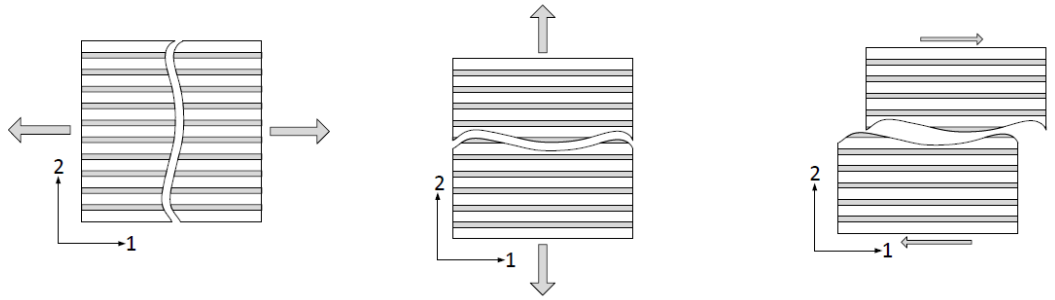

(a) Mode I fracture perpendicular to the fiber direction (b) Mode I fracture parallel to the fiber direction (c) Mode II fracture parallel to the fiber direction

Figure 1: Intralaminar fracture modes in a unidirectionsl fiber reinforced composite laminate[2].

II. Tests on $[90_2/0_2]_S$ Specimens with a Single Edge Notch

In an effort to determine the intralaminar fracture toughness property under tensile loading in the direction of fibers, G_I^{Fiber}, a Single Edge Notch Tension Test (SENT) was carried forth on a cross-ply laminate, $[90_2/0_2]_S$ that is made of an IM7/8552 material system. This test was used in conjunction with an inverse analysis utilizing a finite element model to arrive at the input parameter, G_I^{Fiber}. The SENT and the corresponding inverse analysis were performed for two different notch lengths, 6.35 mm and 12.7 mm, to investigate the existence of dependencies of the fracture property on the notch length.

A. Test Setup

The set of tests to be discussed in this section were all carried forth on SENT specimens with geometries illustrated in Figure 2. The specimen was 254 mm × 50.8 mm characterized by a thin notch at the midpoint of the longside of the specimen. The notch was of variable length, 12.7 mm or 6.35 mm, henceforth referred to as SENT A and SENT B, respectively. These were the only geometric variations between the two sets of tests. Both sets of quasi-static SENT tests were carried out on a displacement controlled test machine. The displacement rate at the grips was specified to be 0.01 mm/s that is slow enough to obtain quati-static responce of test specimens. Figure 3 shows a typical test configuration for the SENT tests performed. Following the insertion of the specimens within the mechanical grips and subsequent placement within the machine, the specimens were slightly preloaded (about 1% of the final complete failure load) to eliminate any initial compliance commonly seen in initially unloaded specimens.

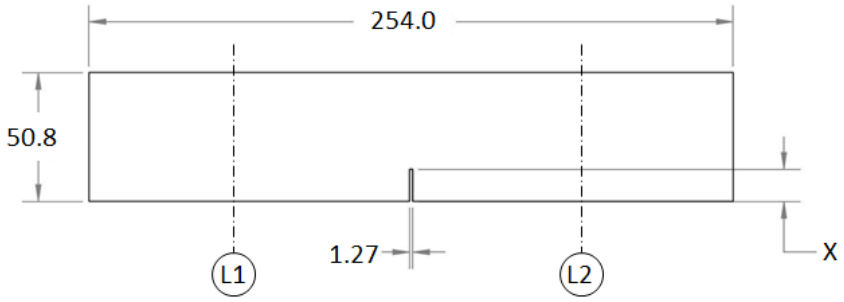

Figure 2: Specimen dimension in millimeters. The notch length, X, is 12.7 for SENT A and 6.35 mm for SENT B.

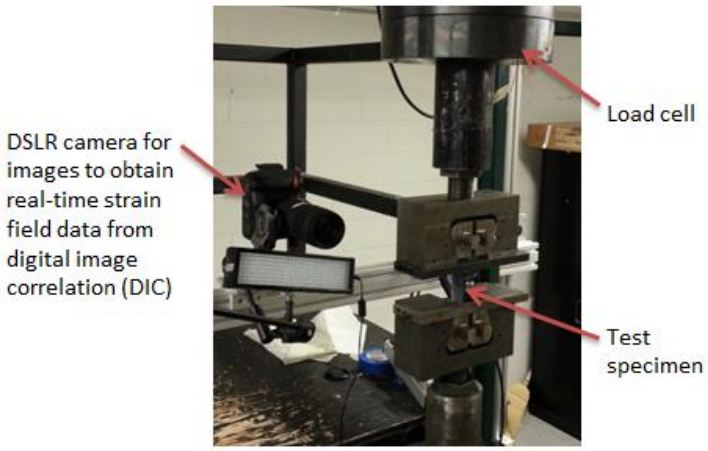

Figure 3: SENT test configuration

In addition to prescribing a displacement rate, and acquiring the displacement and load data obtained from the test machine, a Digital Image Correlation (DIC) system was implemented which allowed for determination of real-time full field strain data. The DIC technique allows for high resolution strain field data on the gauge area of the specimen[1]. In order to use the DIC technique, specimens were sprayed with a contrasting random black and white speckle pattern. By cataloguing the movement of the speckle pattern throughout the duration of the test, and using a post-processing DIC software, ARAMIS, the displacement and strain fields were measured. A digital Nikon D2X body camera was placed directly in front of the specimen focused on the gauge section of the specimen, as shown in Figure 3, so as to record the speckle pattern evolution throughout testing. To maximize resolution, a camera lens of 180 mm focal length was chosen. Additionally, the camera was set to record images at a frequency of 1 Hz.

B. Experimental Results and Discussion

The SENT A test for the $[90_2/0_2]_S$ cross-ply stack-up with the notch length of 12.7 mm showed fairly consistent results. The stress vs. strain data results shown in Figure 4 are macroscopic values chosen to demonstrate the material system behavior on a macroscopic level. The axial stress plotted on the *y*-axis is the load data divided by the measured cross sectional area of the SENT A specimen (1.52 mm × 50.8 = 77.2 mm^2). The strain data evaluation was slightly more involved. To arrive at the macroscopic axial strain data, the ARAMIS software was implemented. Using ARAMIS, the displacement field in the gauge area between L1 and L2 in Figure 2 was determined. Following which, two distinct end displacements at L1 and L2 were resolved by averaging the point wise displacement data over thin strips of pixels on the lines at L1 and L2. Subsequently, the difference between those two values were taken and normalized by their original distance of separation. This process is mathematically surmised as

$$\epsilon_x = \frac{\Delta L}{L} \tag{1}$$

where ϵ_x is the macroscopic axial strain, ΔL is the difference of the axial displacements between L1 and L2 and L is the original distance from L1 to L2.

Figure 5 shows a typical full field strain data overlaid with the specimen images at various points during the test as indicated in Figure 4. Initially a strain concentration began to intensify at the notch tip until the outer layer became nearly saturated with transverse matrix cracks (see Image (b) in Figure 5, where these cracks are indicated as "yellow" vertical bands). At this point, the strain concentration at the crack tip began to slowly prorogate across the specimen. In addition to the crack propagation, the outer layers (90^o layers) fail by transverse matrix cracking as shown in Image (b) of Figure 5. At this stage, the fibers in the axial direction (0^o layers) still remained intact. Finally, as the crack that had been initiated from the notch tip, progressed to about 70% the width of the specimen, the specimen experienced a sudden mixed mode failure (see Image (c) in Figure 5). This mixed mode failure was characterized by fiber pullout and fiber breakage in 0^o layers.

Similar observations of modal failure were also seen in the tests on SENT B specimens that has a notch length of 6.35 mm, albeit with different stress and strain values. The overlay of these results is viewable in Figure 7. Finally, from the data in Figure 4 and Figure 6, several critical values for the SENT tests were calculated and they are compared in Table 1.

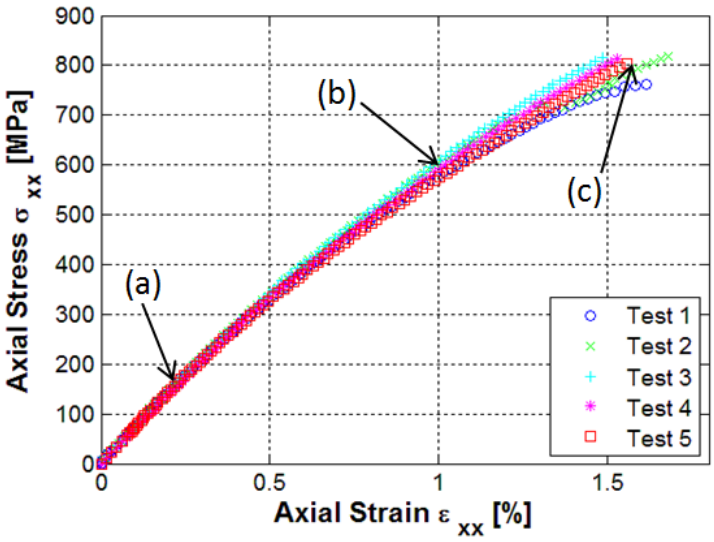

Figure 4: Stress vs. strain data of SENT A specimens

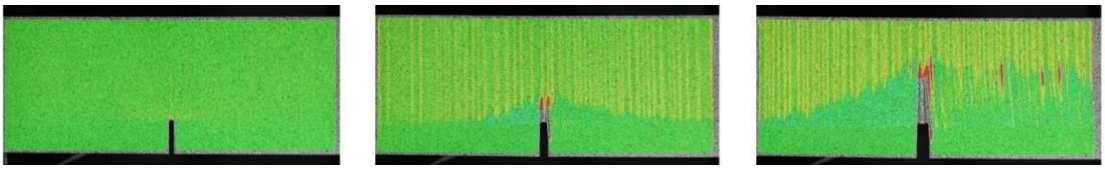

(a) (b) (c)

Figure 5: Typical full field strain data at the points indicated in Figure 4. Image (a) shows the strain developemnt of notch tip strain concentration. Image (b) shows outerlayer crack saturation and Image (c) shows strain field just prior to load drop.

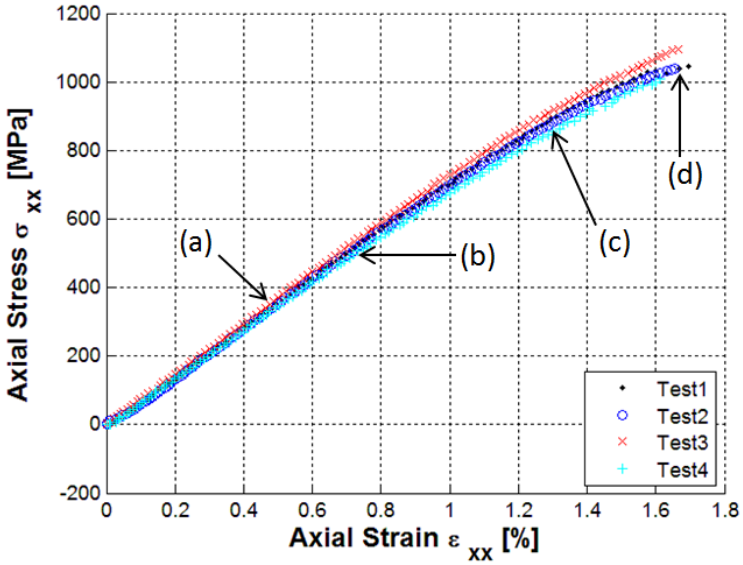

Figure 6: Stress vs. strain data of SENT B specimens

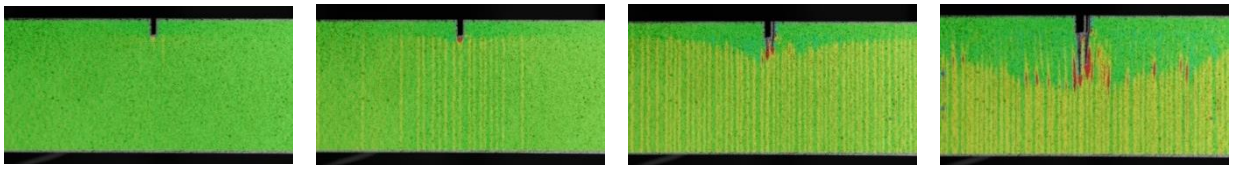

(a) (b) (c) (d)

Figure 7: Typical full filed strain contour for the SENT B test. Image (a) shows beginning of crack development in outer layer. Image (b) shows the increased outer layer crack development. Image (c) exhibits the beginning of crack growth from the notch. Image (d) displays the strain field just prior to load drop.

	SENT A	SENT B
Failure stress (MPa)	802.7±2.3	1051.1±36.7
Failure strain (%)	1.57±0.07	1.67±0.04
Strain at crack initiation (%)	0.36±0.07	0.39±0.11
Initial stiffness (MPa)	72.4±1.8	72.4±1.5

Table 1: Comparison of the critical values from the SENT tests

III. Simulation of SENT tests

The SENT test on $[90_2/0_2]_S$ was aimed at determination of G_I^{Fiber}. G_I^{Fiber} cannot be arrived at directly from the test data. In order to determine this property, one must first carry forth an inverse analysis using finte element analysis (FEA). The process is as follows: 1) execute a set of SENT tests 2) glean the stress and strain data from the experiment 3) change the input G_I^{Fiber} in the FEA simulation until the stress vs. strain data of the simulation aligns with the experimental data. This inverse analysis ultimately led to the determination of G_I^{Fiber}, and shall be discussed in this section.

A. Enhanced Schapery Theory

Enhansed Schapery theory (EST)[3] is capable of modeling the constitutive behavior of fiber-reinforced composite laminates over the full spectrum including damage and failure. Here, the damage is considered as a mechanism that is responsible for material nonlinearity before the material reaches a critical state. Failure is defined as the post-peak softening behavior until the material completely loses stiffnesses. Schapery theory (ST)[4] has been proven to be an accurate and effective homogenized model for progressive damage analysis of laminated composites that exhibit nonlinear behavior due to matrix microcracking[5,6]. As the damage is accumulated, the material starts to lose its strength and cannot carry any more loads. EST combines ST with Crack Band model[7], so that the material failure can be also accounted for.

Figure 8 schematically shows the concept of the modeling strategy of EST. As shown in Figure 8(a), Schapery theory decomposes the total energy into the dissipated energy, S, due to matrix microcracking and the elastic strain energy, W_E. Figure 8(b) shows that the Crack Band model is capable of computing the release of the fracture energy, G_C, over a characteristic dimension. Figure 8(c) illustrates EST that combines ST and Crack Band in order to describe the material behavior over the full range. L_{el} in Figure 8(c) is the characteristic length that ensures the same rate of energy release due to fracture per unit area[3,7].

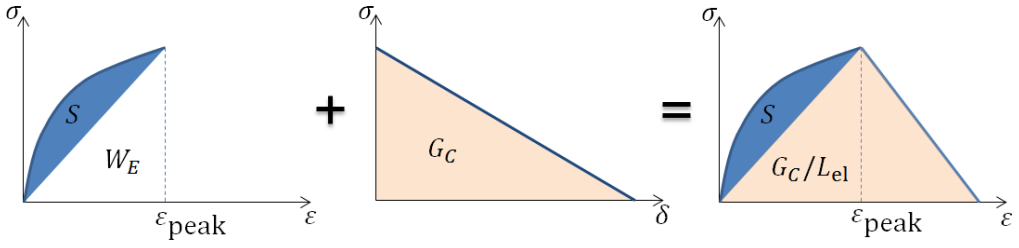

Figure 8: Theoretical background of the enhanced Schapery theory (EST).

B. Input parameters of EST for SENT $[90_2/0_2]_S$ Simulation

EST requires numerous modeling parameters to fully describe the damage and failure behavior of unidirectional fiber reinforced composites. Basic linear elastic lamina properties of IM7/8552 are listed in Table 2. As shonw in Figure 8(a), the damage variable, S, is responsible for the degradation of the stiffnessess, E_{22} and G_{12}. ST characterizes the degrading stiffnesses as functions of S that can be obtained from tensile coupon tests on $[90]_8$ and $[+45_2/-45_2]_S$ laminates for E_{22} and G_{12} respectively. The data for the damage functions are shown in Figure 9. From the $[90]_8$ coupon tests, the failure strain (ε_{peak} in Figure 8) cab be also measured and it is 0.008 mm/mm. Since experiments reveals that 90° layers fail by transverse matrix cracking before fibers in 0° layer are broken as shown in Figure 5 and Figure 7, it is assumed that the failre strain in the transverse direction is only required to initiate the in-plane failure on 90° layers for SENT simulation. After the failure is initiated, the post-peak softening behavior is predicted by an overstress toughness value as shown in Figure 8(b). The overstress toughness value corresponding to the matrix transverse cracking (see Figure 1(b)) is assumed to be the same as the interlaminar fracture toughness value for Mode I that can be obtained from standard double cantilever beam tests. The fracture toughness value of the material system measured from DCB tests is 0.384 N/mm.

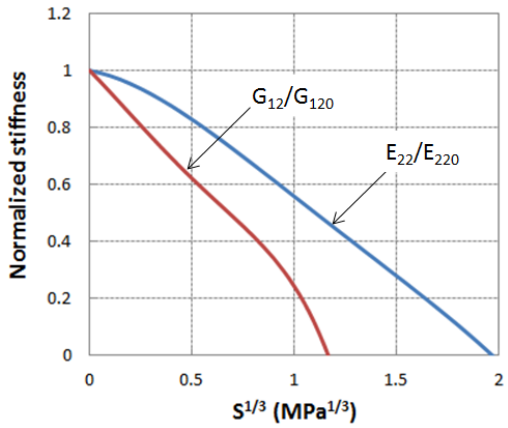

Figure 9: E_{22} and G_{12} as a function of the damage variable, S. E_{220} and G_{120} are the virgin properties before the material is damaged.

Property	Value
E_{11} (GPa)	131.1
E_{22} (GPa)	7.2
G_{12} (GPa)	4.8
ν_{12}	0.34

Table 2: Properties of IM7/8552 material system

C. SENT $[90_2/0_2]_S$ Simulation

The SENT simulation is performed using ABQUS/Explicit with EST implemented via user material subroutine. The specimen is modeled with S4R shell elements with very fine meshes around the notch tip as shown in Figure 10. Since the complete failure of the SENT test is due to fiber breakage on 0° layers, the critical strain, X_{fiber}, that initiates the fiber failure and the corresponding fracture toughness value, G_I^{fiber}, can be obtained by matching the failure strain values reported in Table 1. In the process of finding the two values, X_{fiber} is first obtained until the macroscopic response of the model starts failing by fiber breakage near the experimentally obtaind macroscopic failure stain values as reported in Table 1. After X_{fiber} is found, G_I^{fiber} can be obtained when the value best represents the catastropic failure that occurs abruptly as observed in the experiments. The results of SENT A test data is first used to find X_{fiber} and G_I^{fiber} using the aforementioned methodology. Figure 11 compares the simulation results against the experimental data of SENT A. As shown in Figure 11, with X_{fiber}=0.03 and G_I^{fiber}=40 N/mm, EST caputres the macroscopic behavior accurately upto final failure.. Figure 12 shows the simulation results for SENT B when the same values are used. Figure 13 shows the typical failure modes on 90° and 0° layers at the peak load for the case of SENT A. As can be seen Figure 13, the response of the SENT specimen that is observed from experiments, are captured reasonably well by EST in a macroscopic homogenized sense.

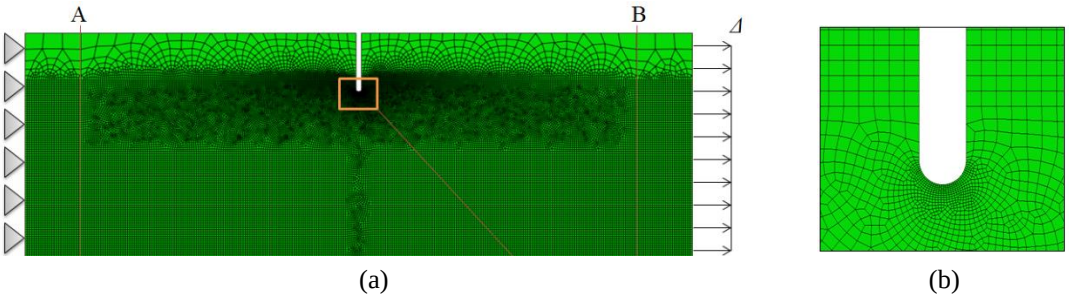

Figure 10: (a) Finite element model for the SENT simulation. (b) Very fine mesh is used around the notch tip.

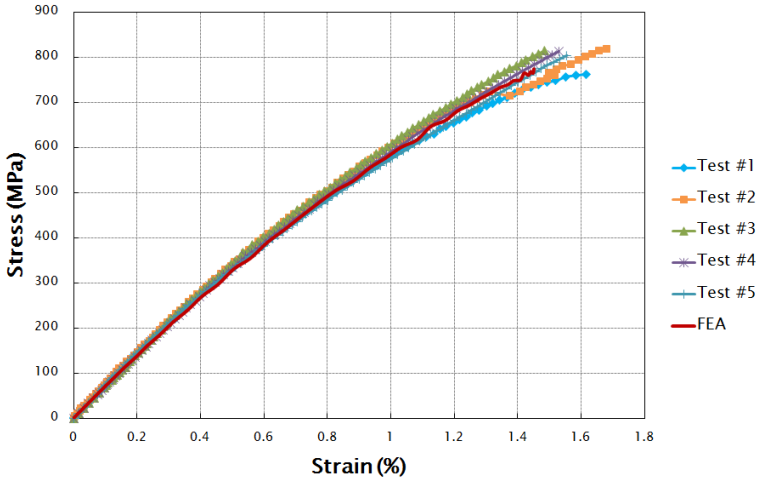

Figure 11: Simulation results for SENT A tests

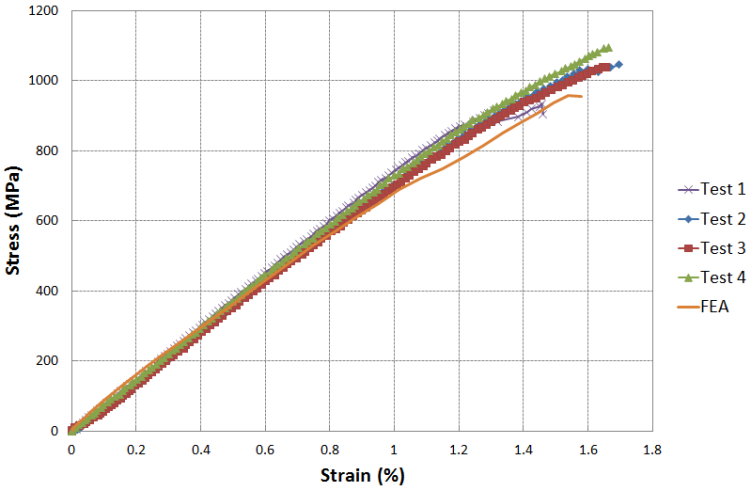

Figure 12: Simulation results of SENT B tests

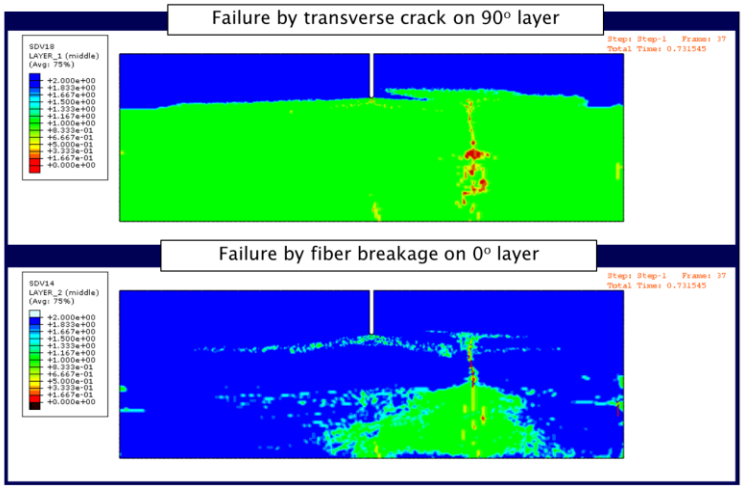

Figure 13: Failure modes on 90° and 0° layers predicted by EST

IV. Conclusion

The SENT test results on cross-ply composite laminates are presented as a means to obtain intralaminar fracture toughness value for the Mode I fiber failure. The tests using DIC techniques provide the detailed information about the failure process on the cross-ply laminate with a single edge notch. The macroscopic stress-strain response of the SENT test is used to measure the in-situ intralaminar fracture properties in conjunction with the FEA model using EST.

Acknowledgments

The authors are grateful for the financial support from the Boeing company.

References

[1]A. Zehdnder, *Fracture Mechanics*, Springer 2012

[2]C. Heinrich and A. M. Waas, Investigation of progressive damage and fracture in laminated composites using the smeared crack approach, 53rd AIAA/ASME/ASCE/AHS/ASC Structures, Structural Dynamics and Materials Conference 2012.

[3]E. J. Pineda and A. M. Waas, Numerical implementation of a multiple-ISV thermodynamically-based work potential theory for modeling progressive damage and failure in fiber-reinforced laminates. International Journal of Fracture 182(1): 93-122.

[4]R. A. Schapery, A theory of mechanical behaviour of elastic media with growing damage and other changes in structure. Journal of Mechanics and Physics of Solids, 38(2):215-253, 1990.

[5]S. Basu, A. M. Waas and D. R. Ambur, Compressive failure of fiber composites under multi-axial loading. Journal of the Mechanics and Physics of Solids, 54:611-634, 2006.

[6]W. Ji and A. M. Waas, Progressive failure analysis for the interaction of interlaminar and intralaminar failure modes in composite structures with an initial delamination. The Aeronautical Journal, 117(1187):71-84, 2013.

[7]Z. P. Bazant and B. H. Oh, Crack band theory for fracture of concrete. Materiaux et constructions. 16(93): 155-177.